Chemical Engineering Journal 520 (2025) 165702

Contents lists available at ScienceDirect

Chemical Engineering Journal

journal homepage: www.elsevier.com/locate/cej

Scalable and sustainable sandwich-structured colorful fabric for passive color-preserving thermal management

Xuexue Xiang [a], Peida Liu [a], Yucan Peng [b], Yao Ma [c], Lijie Du [c], Jing Gao [a,*], Fujun Wang [a], Lu Wang [a]

[a] Shanghai Frontiers Science Center of Advanced Textiles, College of Textiles, Donghua University, Shanghai 201620, China
[b] Department of Energy and Resources Engineering, College of Engineering, Peking University, Peking 100871, China
[c] Benecke Changshun Auto Trim (Zhangjiagang) Co., Ltd., Zhangjiagang 215600, China

ARTICLE INFO

Keywords:
Thermal management fabric
Colored radiative cooling
Hierarchical morphology
Phase change materials

ABSTRACT

Passive daytime radiative cooling fabrics, characterized by high solar reflectance and thermal emissivity, exhibit zero-energy cooling performance under direct sunlight in a sustainable manner. However, these fabrics are predominantly white to maximize solar reflectance, limiting their suitability for applications requiring diverse colors, especially dark ones. In this study, we developed a sandwich-structured fabric (SSF) that combines color-preserving radiative cooling and latent heat storage properties through heat transfer design, effectively minimizing the net heat gain of colored fabrics from the external environment. The SSF features a specific visible reflectivity and high near-infrared reflectivity owing to the integration of the near-infrared transparent colored surface layer and the radiative cooling thermal insulation layer with micro-nano hierarchical structure, while the absorbed heat is further stored as latent heat, enabling efficient thermal management performance. It not only offers significant thermal buffering against temperature increases but also maintains a cooling effect of 4.0–16.0 °C under intense sunlight compared to conventional fabric with the same color. Notably, the black SSF achieves an average temperature reduction of ~10.4 °C under an average solar irradiance of 549.4 W/m^2. Furthermore, the SSF is fabricated through a simple, low-cost, scalable, and environmentally friendly process and exhibit excellent practical performance, paving a powerful way for efficient thermal management of colored fabrics.

1. Introduction

In recent years, climate deterioration driven by global warming and rising energy consumption have garnered global attention [1]. Consequently, research on energy-saving technologies and greenhouse gas emission reduction has become a key focus across various fields, such as materials and construction [2,3]. In particular, passive cooling technologies that reduce cooling energy consumption without relying on conventional active methods have emerged as a promising strategy. Passive daytime radiative cooling involves the spontaneous reflection of sunlight within the wavelength range of 0.3 to 2.5 μm and the emission of thermal radiation through the atmospheric transparent window (ATW; 8 to 13 μm) into ultracold outer space (~3 K), resulting in zero-energy cooling under direct sunlight [4–6]. Based on this principle, a wide range of chemically engineered structural materials, including photonic crystals [7,8], thin films [9–11], coatings [12–14], glass [15], wood [16], ceramics [17], and fabrics [18–20], have been developed for passive daytime radiative cooling to achieve efficient thermal management for extensive daily and industrial applications. Among these, fabrics for daytime radiative cooling are particularly promising due to the widespread use of textile materials in various fields and practical scenarios, offering a potential solution to both global warming and the growing energy crisis.

Radiative cooling fabrics have subsequently emerged in various forms, including woven fabrics [21–23], electrospinning nanofiber membranes [24–26], coated fabrics [27–29], and nonwoven fabrics [30–32], all aimed at integrating radiative cooling functionality into textile materials to achieve effective thermal management in diverse application scenarios. However, most radiative cooling fabrics typically exhibit a super dazzlingly white appearance to maximize cooling performance, which compromises aesthetics and causes visual discomfort, thereby limiting their suitability for outdoor textile applications and

* Corresponding author at: College of Textiles, Donghua University, Shanghai 201620, China.
E-mail address: gao2001jing@dhu.edu.cn (J. Gao).

https://doi.org/10.1016/j.cej.2025.165702
Received 29 April 2025; Received in revised form 30 June 2025; Accepted 5 July 2025
Available online 10 July 2025

restricting their practical use in real-world applications [33]. For instance, in applications such as automotive interiors, transportation seating, tents, roofing, and awning materials, color and appearance are crucial and in significant demand. However, these colorful materials usually absorb more solar radiation, leading to elevated surface temperatures under intense outdoor sunlight, thereby creating harsh thermal environments and discomfort. Especially for automotive interior materials, the selective transmission characteristics of window glass (transmitting shortwave but blocking longwave radiation) inhibits internal heat exchange, causing a typical "greenhouse effect" [34]. This not only significantly reduces thermal comfort but also poses major safety risks [35,36]. Studies have shown that interior surfaces are key factors in creating the greenhouse effect and determining the interior temperature, and they account for most air conditioning energy consumption [37]. Therefore, the key technical challenge lies in developing materials that can effectively reduce solar heat gain while maintaining their color appearance. This is particularly important in practical applications to improve thermal comfort and reduce cooling energy consumption.

To enhance human thermal comfort and conserve energy, colored radiative cooling fabrics (CRCFs) have been explored [38–40]. Such as photonic crystals [41], structural color fabrics [42], electrospinning membranes [43], porous-coated fabrics [44], and spray-coated fabrics [45], but their performance and application scope are still limited. For instance, photonic crystals and structural color fabrics are costly and challenging. Furthermore, although colored electrospinning membranes and porous coated fabrics offer high cooling performance, they cannot maintain their original color appearance well due to internal porous scattering, making it difficult to achieve effective thermal management for dark or black appearances. Their complicated, high-cost, and solution-processed syntheses involving toxic solvents (adversely affecting human health and the environment) limit their mass production. Moreover, spray-coated fabrics require improved scalability and reliability for practical application. Therefore, developing efficient radiative cooling fabrics that meet different color appearance requirements in a simple, low-cost, and highly scalable manner is critical and presents a significant challenge [46].

For colored radiative cooling, the fabric will inevitably absorb heat from visible solar light and heat transfer via non-radiative mechanisms such as conduction and convection, causing an increase in the fabric's surface temperature. Phase change materials (PCMs), due to their superior heat storage properties, have been extensively applied and researched in the fields of energy storage and thermal management [47–49]. Integrating these materials with fabrics can enhance their added value by endowing them with dynamic temperature regulation capabilities. However, limited by the enthalpy and dosage of phase-change materials, phase-change fabrics (PCF) primarily provide a buffering effect under thermal stimulation, and the end of phase-change heat storage process under the thermal load of long-time outdoor exposure to solar radiation does not have a more significant impact on the temperature of the fabric after reaching thermodynamic equilibrium. Thus, combining it with other thermal management methods is a practical approach to enhancing thermal management performance [50,51].

Herein, we present a simple, low-cost, environmentally friendly, and scalable approach to fabricate a colored sandwich structured fabric (SSF) that meets the thermal management demands for outdoor colored fabric applications, the preparation process is shown in Fig. S1. We engineered the SSF by integrating a near-infrared transparent colored

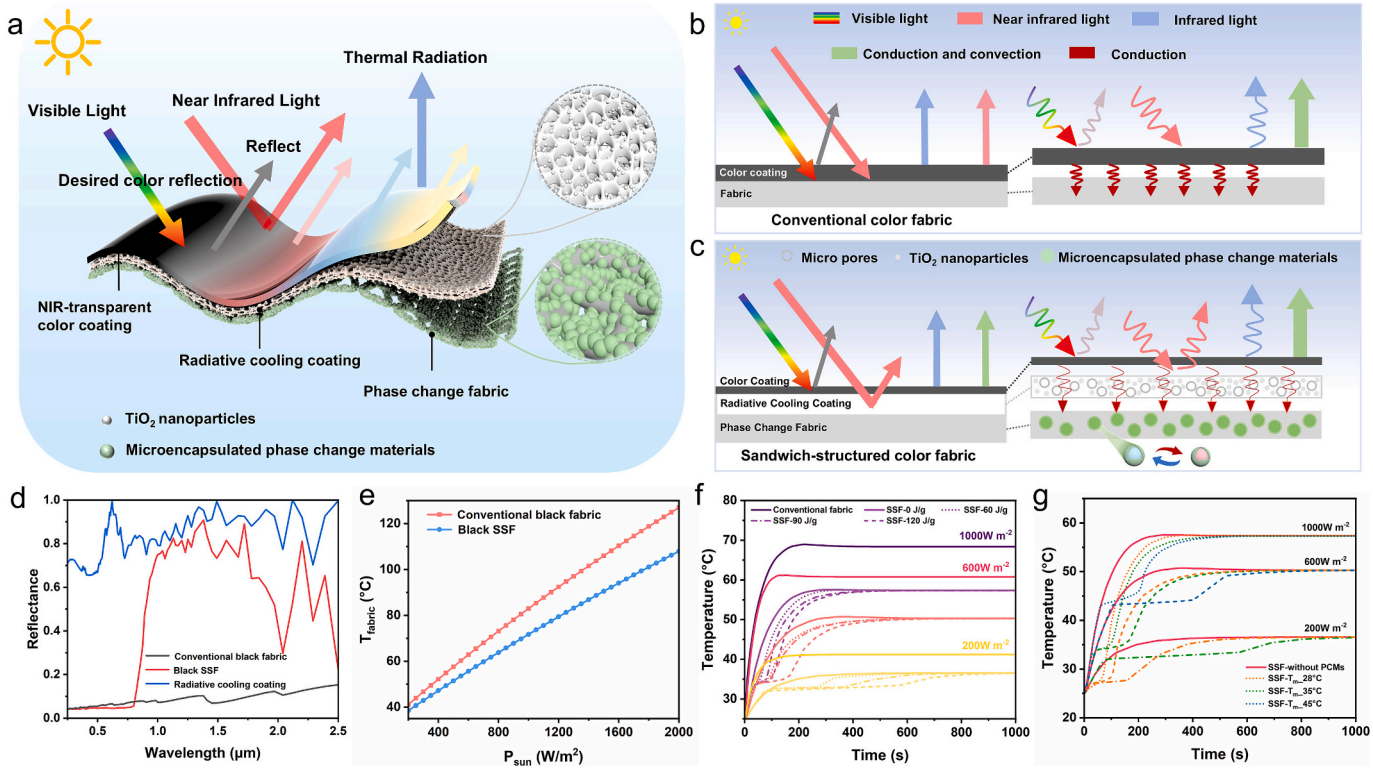

Fig. 1. Design and model calculations of the sandwich-structured colored fabric (SSF). (a) The structure of the SSF is composed of a colored top layer, radiative cooling thermal insulation layer, and phase change fabric. (b and c) Schematic showing the interaction of sunlight with conventional coated fabrics (b) and SSFs (c), respectively, and the heat transfer pathways. (d) FDTD simulated reflectance of conventional black fabric, black SSF, and radiative cooling coating. (e) Calculated thermodynamic equilibrium temperatures of the conventional black fabric and the black SSF under different solar radiation intensities. (f) Calculated temperature variation of the commercial black fabric and the black SSF with different PCMs' content under different solar radiation intensities. Purple: 1000 W/m^2; red: 600 W/m^2; yellow: 200 W/m^2. The T_m is fixed at 35 °C. (g) Calculated temperature variation with the T_m evolution under different solar radiation intensities and the calculated buffer time can be found in Supporting Information. (For interpretation of the references to color in this figure legend, the reader is referred to the web version of this article.)

top layer, a radiative cooling thermal insulation middle layer, and a bottom phase change fabric (PCF) into a multilayer fabric (Fig. 1a). The top layer features specific visible reflectivity, high near infrared (NIR) transmittance, and high infrared emissivity by incorporating NIR transmissive colorants into a visibly transparent polymer matrix of polyvinyl chloride (PVC). The radiative cooling thermal insulation layer is created by randomly embedding TiO_2 nanoparticles into the PVC matrix via physical foaming, yielding a hierarchical structure with microporous and nanoparticle-integrated characteristics that enable the strong reflection of solar radiation transmitted by the top layer and further reduce heat input. Furthermore, the bottom fabric layer containing phase change microcapsules absorbs and stores inner heat to delay temperature increase. This customization of heat transfer pathways maximizes thermal management in colored fabric. With this design, the SSFs exhibit almost identical colors and visible reflectance to those of commercial colorful fabrics, but a considerably higher near-infrared reflectivity, lower thermal conductivity, and excellent thermal storage properties. Consequently, they not only significantly slow down the heating rate, but also exhibit substantially lower temperatures under sunlight. In addition, it also has superior applicability and could be industrially produced via a roll-to-roll process at high speed, bridging the gap between theoretical research and actual product development.

2. Results and discussion

2.1. Concept design and theoretical analysis of the SSF for colored thermal management

We compared the concept and structural design of SSFs with conventional fabrics in the same colors, and analyzed the heat transfer and thermal performance with numerical simulations and theoretical calculations, as shown in Fig. 1. Fig. 1b illustrates the heat transfer mode of conventional colored coated fabrics under solar radiation: the top layer absorbs part of the solar visible light (displaying the corresponding color) and almost all of the NIR light. Heat is transferred from the exterior to the interior and balanced between input and output via the fabric's surface thermal radiation dissipation and heat exchange with the external environment through conduction and convection. However, the NIR light, which accounts for approximately 51 % of solar radiation and is unrelated to color performance, should be maximally reflected to minimize the solar heat absorbed by the fabric. Higher NIR reflectivity results in a greater temperature reduction (Fig. S2). As shown in Fig. 1c, the heat transfer mode of SSFs shows that the visible wavelengths complementary to the desired color are absorbed by the top layer, while the NIR radiation, is transmitted through the top layer and highly reflected by the intermediate radiative cooling layer. The hierarchical morphology of micropores and nanoparticles in the radiative cooling layer provides high reflectance and excellent insulating properties, reducing the heat transfer (from the color top layer) and accumulation within the fabric. Moreover, the bottom PCF can absorb and store heat transferred through the insulation layer at specific temperatures, thus delaying the fabric's temperature rise. Here, we calculated the heat transfer and corresponding temperature changes during both transient and steady-state heat transfer for the two fabrics with differing optical and thermal properties, and the heat transfer model is shown in Fig. S3. Further details of theoretical analysis can be found in the Supporting Information.

To elucidate the thermal management properties of SSFs, we take the black-coated fabric with the highest thermal management demand as an example, using the model mentioned above and with the conventional black-coated fabrics as the control. Finite-difference time-domain (FDTD) simulations show that the black SSF exhibits significantly higher reflectance in the NIR region than the conventional fabric (Fig. 1d), thereby reducing the solar radiation heat input into the fabric. Correspondingly, the calculated thermodynamic equilibrium temperatures of the SSFs are always much lower than the conventional coated fabrics with the same color under various solar radiation intensities (Fig. 1e), and this temperature management effect becomes more pronounced with increasing solar intensity. Meanwhile, the calculated temperature difference between the two fabrics decreases with increasing heat transfer coefficient (Fig. S4), which is because that higher heat transfer coefficient results in a more intense heat exchange with the external environment, thus decreasing the temperature difference between the two fabrics mainly caused by the difference in absorbed radiant heat. The simulated temperature change curve also confirms the reduction of the thermal equilibrium temperature under various solar radiation intensities (Fig. 1f). Moreover, during the transient heat transfer process before reaching thermodynamic equilibrium under a fixed solar irradiation intensity, according to Eq. S16, the fabric's latent heat of fusion increases with the PCMs content, prolonging the phase change duration and progressively improving the heat-time transfer in temperature rise process. Owing to the decreased heat input, the lower solar radiation power density exhibits the longer storage time of the PCMs correspondingly, leading to a better temperature delay effect for the fabric.

The phase transition temperature (T_m) significantly influences the heat transfer process in composite fabrics, affecting their thermal efficiency and playing a critical role in temperature rise buffering. Simulations were conducted to analyze the temperature rise curves of fabrics with different T_m during the heat transfer process (Fig. 1g). Under solar irradiation, the fabric's surface coating absorbs solar heat, and it is evident that a lower T_m at the fabric's bottom initiates temperature buffering at a lower level, improving heat transfer efficiency. However, due to the substantial heat input, the temperature rise rate is faster, resulting in a shorter duration of temperature rise delay. Moreover, decreasing the solar radiation intensity and incorporating additional radiative cooling properties can effectively reduce external heat input, thereby prolonging the working time of PCMs and enhancing the heat-time transfer effect (Fig. S5). Increasing the T_m extends the duration but raises the buffering temperature. To optimize the performance of thermal management fabrics, PCMs with lower melting points but higher than ambient temperatures should be considered under the premise of compromising and satisfying thermal buffering requirements [52]. Hence, comprehensive consideration should be given to realistic scenarios and needs during design and application.

2.2. Materials characteristic

To achieve sustainable and scalable colored thermal management in SSFs, PCF was first prepared via an industrial dip-rolling process. Then, polymer-coated composite fabrics were prepared using a massively scalable coating technology. Due to the superior mechanical properties, flexibility, high transparency, strong compatibility, and intrinsic infrared resonance of C—C, C—H, and C—Cl bonds within the ATW [53], PVC was selected as the polymer matrix embedded non-absorbent colorants to create a near-infrared transparent colored surface layer with an excellent thermal emission capacity, and then a large number of micropores were generated in the polymer coating and compounded with high refractive index TiO_2 nanoparticles to form a micro-nano hierarchical morphology by physical foaming technology to obtain a radiative cooling coating. Alkanes with high phase change enthalpy and tunable T_m were used as the PCMs, and widely available, heat-resistant polyurethane (PU) was chosen as the encapsulation medium. The PCMs were encapsulated into dimensionally stable, durable microcapsules (mPCMs) to prevent leakage, and PCF was subsequently prepared using the dip-rolling process. The scraper-coated PVC layer was laminated with the PCF to form the colored sandwich-structured fabric. This facile process yielded coated fabrics with various colored surfaces (Fig. 2a-1), featuring a green and straightforward production process without harmful solvents or by-products. The thickness can be easily controlled by adjusting the scraper distance, and the process can be easily scaled up for continuous mass production using industrial coating and lamination techniques (Fig. 2a-2). For ease of exploration, take the black-coated

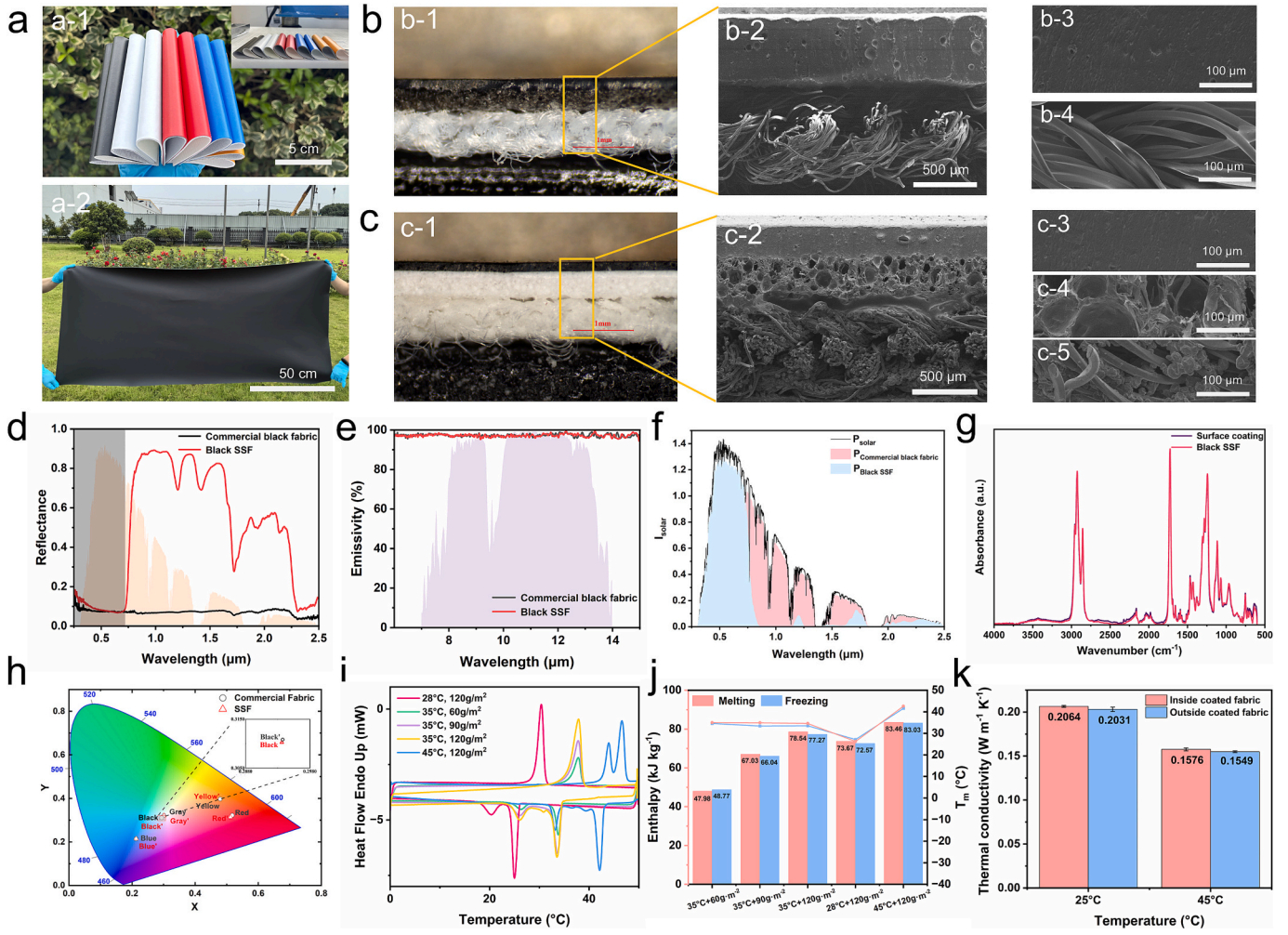

Fig. 2. Structure, optical properties, and thermal properties of the SSF. (a) Optical photographs of commercial coated fabrics and SSFs in different colors. (b–c) SEM images of the different positions inside the commercial black coated fabric (b) and the black SSF (c), including colored top coating (b-3 and c-3), radiative cooling thermal insulation coating (c-4), and bottom fabric substrate (b-4 and c-5). (d–e) Reflectance in the solar spectrum (0.25 to 2.5 μm) (d) and emissivity in the atmospheric window (8 to 13 μm) (e) of the commercial black coated fabric and black SSF. (f) Calculated absorbed solar heat of commercial black fabric and black SSF. (g) FTIR absorbance spectrum of the surface coating and black SSF. (h) Color space of the commercial fabric and SSFs in different colors (black, gray, red, blue, yellow). (i) DSC curves of heating and cooling processes for PCF with different PCMs. (j) Enthalpy and phase transition temperature of PCF during the melting and freezing process. (k) Thermal conductivity of the black SSF before and after melting.

fabric as an example, with relevant data for other colors included in the Supporting information. As shown in Fig. 2b and c, with the element distribution depicted in Fig. S6, compared to the two-layer structure of the conventional black fabric, the black SSF exhibits a distinct three-layer structure. The top layer comprises a dense PVC polymer coating that imparts the desired appearance and excellent hand feeling. The radiative cooling layer, with randomly distributed micropores and nanoparticles, demonstrated a hierarchical structure that provides high solar reflectance and reduced thermal conductivity. The bottom layer features microencapsulated phase change materials (mPCMs) attached to the fiber, offering mechanical support and thermal storage properties. These structural characteristics confirmed the successful development of SSFs with micro-nano hierarchical structures and specific heat transfer pathways in a sandwich configuration.

To evaluate the radiative properties of the SSF, the optical properties, including the solar radiation range (0.3 to 2.5 μm) and the ATW range (8 to 13 μm), were experimentally investigated (Fig. 2d and e), and we further calculated the absorbed solar radiation power based on the reflectance within the solar spectrum (Fig. 2f). The pure PVC coating demonstrated a transmittance of over 95 % in the solar spectrum (Fig. S7a and b), indicating low intrinsic absorption and high transparency when exposed to solar irradiation. With this advantage, the fabric retained its NIR transmittance by incorporating non-absorbent colorants in the NIR region while presenting the desired color. With the hierarchical structure of micropores and nanoparticles, the radiative cooling layer at the bottom exhibits strong Mie scattering, resulting in a high solar reflectance (Fig. S7e). For example, the PVC coating compounded with near-infrared transparent black colorants has specific absorption properties in the visible light region of the solar spectrum to display the corresponding color (Fig. S8c) and high transmittance in the NIR region (Fig. S7d), which facilitates the transmission of NIR radiation through the top layer to be effectively reflected by the underlying radiative cooling layer, thus achieving a high NIR reflectance (Fig. S7e). At the same time, the fabric maintains a high emissivity in the ATW range (Fig. S7f). Similarly, the solar spectrum characteristics of other colored top layers also exhibit non-absorbent properties (Fig. S8). The process parameter optimization for colorants and TiO_2 is illustrated in Fig. S9. The black SSF with optimized coatings laminated with phase change energy storage fabrics could reflect up to 90.50 % in the NIR region (Fig. 2d). In contrast, due to carbon black colorants' high solar spectrum absorption (Fig. S10), conventional black-coated fabrics exhibit only 5.73 % reflectance (Fig. 2d). Consequently, the black SSF

absorbs significantly less solar radiation power in the NIR band than conventional black fabrics (Fig. 2f), with a difference ΔP of 304.50 W/m^2. Other colored SSFs (gray, red, blue, yellow) also exhibit high NIR reflectance and reduced solar absorption power by 54.86, 306.31, 95.94, and 52.33 W/m^2, respectively (Fig. S11), suggesting that the sandwich structure thermal management strategy applies to various colors and can significantly decrease absorbed solar radiation. Furthermore, all colored top layers, conventional fabrics, and SSFs demonstrate an emissivity exceeding 96 % in the ATW region (Fig. 2e, Fig. S12–13 and Table S2), deriving from the intrinsic resonance of chemical bonds within the surface coating (Fig. 2g). Accordingly, we calculated the thermal equilibrium temperatures of the aforementioned commercial fabrics and SSF fabrics with identical colors under varying solar radiation intensities and convective heat transfer coefficients (h_c). As illustrated in Figs. S14 and S15, the SSF fabrics are significantly cooler than the commercial fabrics. Meanwhile, T_{amb} was fixed as 30 °C and h_c was chosen as 0, 4, 8, 12 W m^{-2} K^{-1}. The calculated theoretical net cooling power of the commercial fabrics and the SSF with the same color (Fig. S16) shows that the SSF exhibits a significantly higher net radiative cooling power than the commercial fabrics. This is attributed to its relatively higher near-infrared reflectance, which corresponds to a reduced solar radiation absorption power. Most importantly, unlike directly incorporating TiO_2 particles into the fabric's coating, which would significantly change the original color appearance and optical properties (Fig. S17), the sandwich structure design does not affect the color appearance of fabrics. The fabric's color remains highly consistent before and after structural application (Fig. 2h and Table S3), which is crucial for aesthetic design and large-scale production.

High-efficiency latent heat storage can delay temperature rise and reduce heat input, as demonstrated by the simulated fabric temperature change process (Fig. 1g and h), with key factors including enthalpy, phase transition temperature, specific heat capacity, and thermal conductivity. With increasing carbon chain length of alkanes within the mPCMs, the T_m of the PCF increase from 28 °C to 45 °C (Fig. 2i and j), and the heat storage enthalpy range from 72 kJ/kg to 83 kJ/kg. The PCF's enthalpy increases with the mPCMs' content. Corresponding thermal energy storage performance of the SSFs is shown in Fig. S18. At the phase transition temperature range, the fabric's specific heat capacity significantly increases due to the heat absorption during the melting of PCMs, which is critical to determine the ease of temperature change on the fabric. Consequently, compared to conventional fabrics, SSFs require more heat input for temperature rise, thus reducing the temperature rise rate and delaying the time to reach thermodynamic equilibrium. To achieve the optimized performance of SSF, the mPCMs with a T_m of 35 °C was selected. Furthermore, considering the fabrication and bonding properties of the actual coated fabrics, the PCF's load weight was determined to be 120 g/m^2. The PCF exhibits high thermal stability up to 220 °C, beneficial for stability during the coating process (Fig. S19). Additionally, the SSF exhibits constant optical properties before and after melting, which guarantees stable cooling performance during the recycling utilization (Fig. S20). Thermal conductivity is crucial in heat transfer and determines thermal diffusion efficiency. With the abundant micropores inside, the radiative cooling insulation layer exhibits significantly lower thermal conductivity than the original dense PVC coating (Fig. S21), which effectively reduces inward heat transfer from the top surface after absorbing solar heat. As for the bottom fabric, as we expected, due to the large number of mPCMs filling the pores inside the fabric, the thermal conductivity of the PCF is significantly higher than that of the blank fabric, which is conducive to the rapid absorption and storage of excess heat conducted into the PCF to slow down the temperature rise. Overall, the composite structural design reduces the thermal conductivity of the composite fabric, and owing to the PCMs transitioning from solid to liquid upon heat absorption [54], the fabric's thermal conductivity decreased after melting (Fig. 2k), thus reducing the inward heat input through the composite fabric.

2.3. Thermal management performance

Indoor simulated experiments and continuous outdoor thermal measurements were carried out to investigate the thermal management performance of the colored SSFs. In the indoor simulation experiment (Fig. 3a and b), xenon lamp was used to simulate solar radiation and the surface temperature was monitored and compared in Fig. 3c and d. When reaching thermal equilibrium, the black SSF remains 12.40 °C cooler than the commercial black fabric under 1000 W/m^2 solar irradiation, consistent with theoretically calculated heat equilibrium temperature (Fig. S15). During the heating process, the black SSF demonstrates a substantial temperature buffer platform at the phase transition temperature, exhibiting an enhanced cooling effect during the initial 10 min with a heightened temperature difference compared to equilibrium. This phenomenon can be attributed to the heat absorption by the PCMs undergoing a phase transition process. Moreover, after the cessation of solar irradiation, the cooling process of the fabric also exhibited a thermal buffering plateau without any temperature increase (Fig. S22). This enables the PCM to continuously provide thermal regulation in a cyclic and sustained manner over extended periods. Furthermore, this advantage is more evident when compared to the thermoregulation effect of commercial black fabric containing PCMs, which is due to the high NIR reflectivity of the black SSF reducing the heat input per unit of time, thereby extending the phase change thermal storage time. Similarly, with solar radiation decreases, the heat absorbed by the fabric surface diminishes, leading to an extended duration of the phase change process in the PCM, which delays the temperature rise from 10 min to 30 min (Fig. S23). Therefore, PCMs can effectively reduce the temperature rise rate, extend the time to thermal equilibrium, and enhance the cooling performance. The high NIR reflectivity not only significantly reduces the thermal equilibrium temperature of colored fabrics, but also extends the duration of phase change thermoregulation. The synergistic effect of phase change heat storage and radiative cooling provides fabrics with optimal thermal management performance. For gray/red/blue/yellow colors, the SSFs remain 5.09 °C, 12.75 °C, 7.00 °C, and 4.66 °C cooler than the commercial fabrics (Fig. S24), respectively, demonstrating the versatility of sandwich-structured thermal management designs for various color appearances. Moreover, this cooling performance is directly proportional to the absorbed power difference resulting from the near-infrared reflectance. To investigate the thermal management potential of SSFs when used as either the exterior roof surface or the interior surface of an enclosed space, we conducted comparative measurements of the internal air temperature under an average solar irradiance intensity of 500 W/m^2 (Fig. S25). The results show that the high near-infrared reflectivity of the SSF effectively reduces the internal air temperature by 3–4 °C. Moreover, the PCMs not only slow down the rise in air temperature but also reduce the peak temperature by approximately 0.5 °C, demonstrating their excellent temperature regulation performance.

To further demonstrate the cooling effect of the SSFs under realistic outdoor conditions, we conducted comparative tests by exposing the SSFs and commercial fabrics to direct sunlight (Fig. 3e and f). Under solar irradiation, temperature curves fluctuated due to real-time changes in weather conditions (Fig. 3g). The surface temperature of the black SSF remained consistently lower than that of the conventional black fabric (Fig. 3h), with a maximum temperature difference of 16.0 °C (Fig. 3i), confirming its strong temperature management capability. The temperature difference fluctuated with the solar radiation intensity, with stronger radiation resulting in a more significant effect. During the initial temperature rise under irradiation, a significant increase in ΔT is observed, which is attributed to the phase change heat absorption that delays the temperature increase upon reaching the phase change temperature. At night, the latent heat released by the phase change is gradually dissipated through convection and radiation, resulting in a smooth temperature decrease (Fig. S26). Additionally, we tested the outdoor temperature change curves for SSFs in other colors

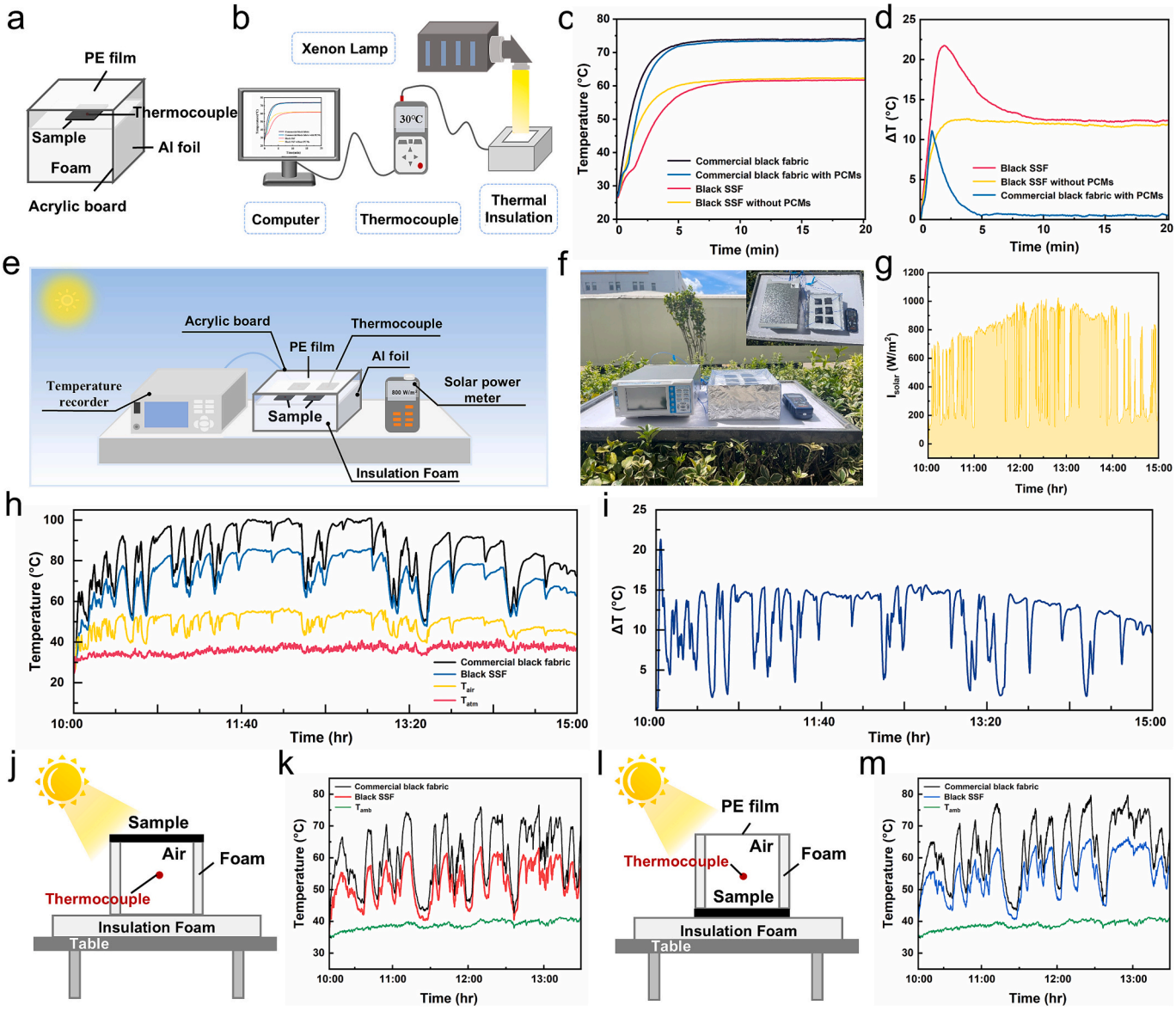

Fig. 3. Cooling performance of the black SSF. (a and b) Schematic diagram (a) and photo (b) of indoor setup for the cooling performance test. (c and d) Temperature comparison of commercial black fabric, commercial black fabric with PCMs, black SSF, and black SSF without PCMs tested indoor (c) and temperature reduction curve (d). (e and f) Schematic diagram (e) and photo (f) of outdoor setup for the cooling performance test. (g) Solar irradiation intensity for outdoor cooling performance test. (h and i) Temperature comparison of commercial black fabric and black SSF tested in Suzhou, China (17 September 2023) (h) and temperature reduction curve (i). (j and m) Schematic diagram of outdoor experiment setup (j) and air temperature comparison (k) for the cooling performance test as roof surface; schematic diagram of outdoor experiment setup (l) and air temperature comparison (m) for the cooling performance test as interior surface, tested in Shanghai, China (25 August 2024).

(Fig. S27), showing reductions of 9.43 °C, 18.04 °C, 9.16 °C, and 8.66 °C for gray, red, blue, and yellow fabrics, respectively. These tests, which isolated heat convection and conduction, effectively simulated the thermal management performance of the fabrics in outdoor enclosed spaces, such as automotive interior materials. Furthermore, to simulate real-world applications such as roofs, awnings, and bicycle seats exposed to outdoor conditions, we conducted simulations incorporating thermal convection and recorded the resulting temperature variations (Fig. S28). Enhanced thermal convection reduced the proportion of radiative heat transfer, leading to a decrease in the temperature difference primarily driven by variations in radiative absorption. However, a temperature difference of approximately 10 °C was still observed. Additionally, the spatial thermal management potential of SSF as both a roof (Fig. 3j and k) and interior surface was evaluated (Fig. 3l and m). Compared to commercial black fabrics, air temperature reductions of up to 15.07 °C and 14.83 °C were achieved in confined spaces, respectively, highlighting the superior thermal management performance of SSFs in diverse outdoor radiation environments.

In summary, this section experimentally verifies that the design of SSFs supports a wide range of colors and delivers excellent thermal management performance across various application scenarios. It further illustrates the synergistic effect of radiative cooling and latent heat storage on the thermal performance of SSFs. Under solar irradiation, the SSF's high NIR reflectivity effectively reduces radiant heat absorption, significantly lowering the thermal equilibrium temperature. The latent heat storage properties of the PCMs provide a temperature buffer, delaying thermal equilibrium. This buffering effect increases as heat input decreases, with both mechanisms working together to achieve efficient thermal management throughout the heating process. Additionally, external environmental factors, such as solar radiation

intensity and air convection coefficients, influence both the thermal equilibrium temperature and buffering effect.

2.4. Evaluation of practical application feasibility

Given the excellent scalability and sustainability of the sandwich-structured thermal management design in this study, we further explored its performance in various real-world applications, as shown in Fig. 4. Fig. 4a compares the appearance of the black SSF with conventional black fabric under different temperature conditions, demonstrating consistent color appearance and stability across low and high temperatures. Thermal infrared imaging reveals that the black SSF maintains a significantly lower surface temperature than the commercial fabric of the same color. We also tested the surface thermal management effects in real-world applications, such as roof canopies, tents, automotive interiors, and bicycle seats. Long-term infrared thermal images indicate that SSFs effectively reduce surface temperature under prolonged exposure to solar radiation and air convection (Fig. 4b). In enclosed car environments, where long-wave thermal radiation from the surface is blocked, the SSF surface still exhibits a significant temperature reduction, which is attributed to its reduced absorption of solar radiation. This demonstrates superior surface thermal management performance and enhances thermal comfort.

The SSFs combine the benefits of a flexible polymer coating and a fabric substrate, offering superior flexibility, mechanical properties, water and dirt resistance, and durability. As shown in Fig. 4c, the black SSF demonstrates exceptional flexibility and compliance, allowing it to bend freely without damage. The fabric retains its original state after bending, ensuring adaptability to various outdoor scenarios. When exposed to contaminants, they easily slide off the surface (Fig. 4d), and

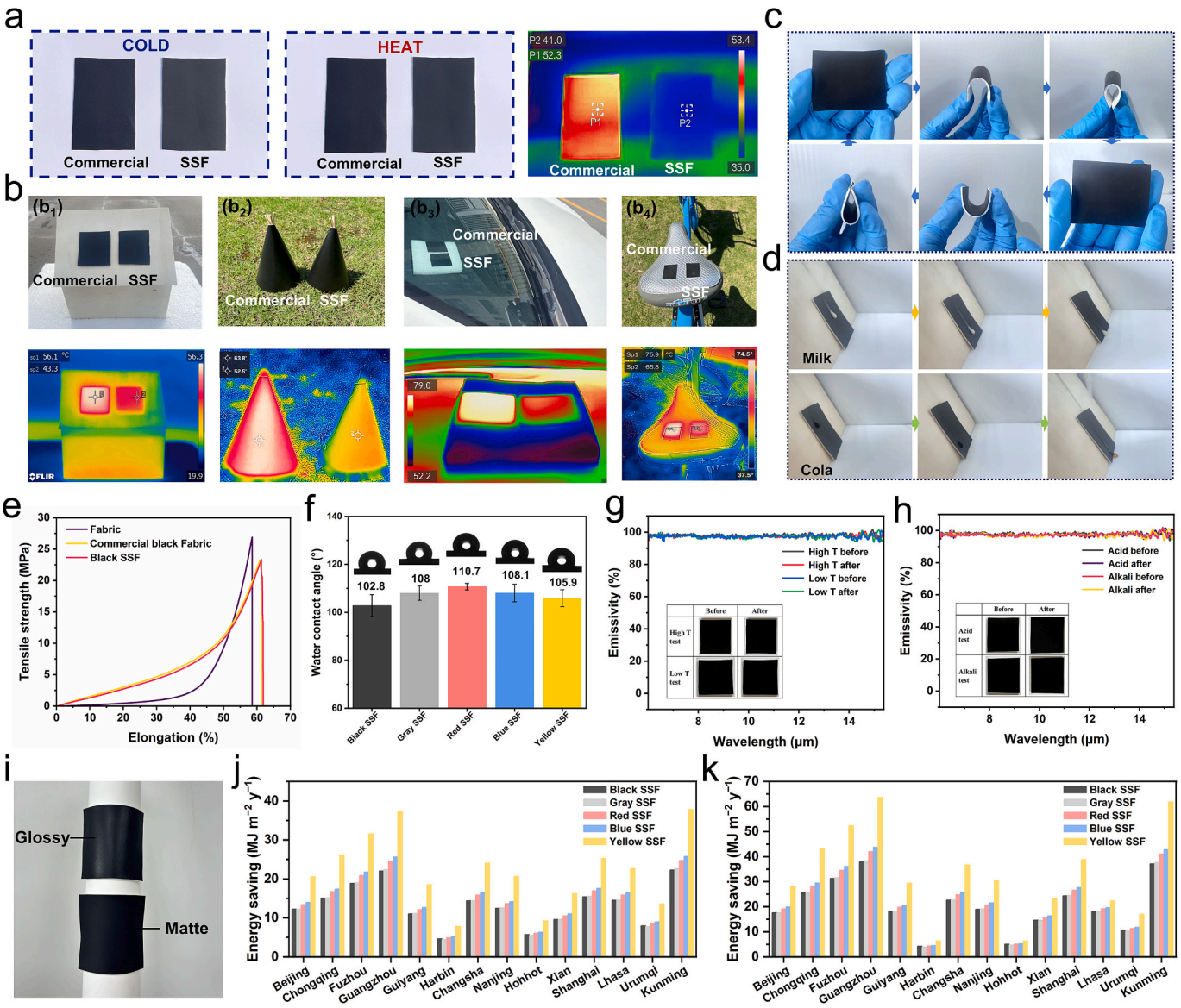

Fig. 4. Evaluation of practical application feasibility. (a) Optical and infrared images of the commercial black-coated fabric and the black SSF. Cold: indoor ambient temperature of 25 °C; heat: after exposure to outdoor solar irradiation for 1 h. (b) Outdoor cooling performance of the commercial black coated fabric and the black SSF, including roof canopies (b_1), tents (b_2), automotive interiors (b_3), and bicycle seats (b_4). (c and d) Flexibility (c) and anti-pollution performance (d) of the black SSF. (e) Mechanical strength tests of the black SSF strength versus elongation. (f) Measured water contact angles for the SSFs in different colors. All the samples show decent hydrophobicity. The error bars indicate the SD values of multiple measurements. (g and h) Measured MIR emissivity for samples before and after the high/low-temperature test (g) and acid/alkali test (h). No noticeable change was observed. The inset exhibits images of samples before and after tests, demonstrating that visual appearance was also retained. (i) By printing glossy and matte polyurethane (PU) inks separately in the top layer, glossy and matte textures can be achieved, respectively. (j and k) Annual energy savings of SSFs used as (j) building roofs and (k) building roofs and exterior walls in 14 typical Chinese cities.

the fabric can be easily wiped clean, restoring it to its original state (Movie S1). Mechanical testing results reveal that the SSF can withstand a tensile force of 23.3 MPa and an elongation of 61.3 % (Fig. 4e), comparable to the commercial one, meeting the high mechanical strength requirements of realistic scenarios. Water contact angle tests demonstrate the excellent water resistance of SSFs, with an average water contact angle of 107.1° (Fig. 4f and Movie S2 and S3), enhancing stability in humid environments. To assess the durability of the SSF, the fabric was stored for one week at high temperature (60 °C), low temperature (−20 °C), acid (sulfuric acid, pH = 4), and alkali (sodium hydroxide, pH = 10) environment. Spectral and thermal storage performance were measured, and the visual appearance of the samples was observed before and after each test. After high and low-temperature tests, the fabric's mid-infrared high emissivity characteristics remained unchanged (Fig. 4g), and solar spectral properties were also unaffected (Fig. S29a), with photographs confirming the coating's intact appearance (inset of Fig. 4g). The optical properties and appearance of the coated samples also remained good after exposure to acid and alkali (Fig. 4h and Fig. S29b). After these treatments, the SSF showed no significant changes in phase change temperature or latent heat (Fig. S30a–b), and its heat storage performance remained highly consistent after 200 thermal cycles (Fig. S30c–d). Moreover, the SSF fabric exhibited excellent spectral stability after undergoing two weeks of accelerated xenon lamp aging and accelerated UV aging (Fig. S31). These results demonstrate that the SSF exhibits excellent environmental adaptability and durability, which is crucial for maintaining spectral and thermal management performance under long-term practical applications.

Furthermore, adopting suitable polymer adhesives on the top surface allows for the presentation of various surface glosses (Fig. 4i), which is challenging for photonic structure design. Optical tests under different gloss finishes indicate that these treatments do not significantly affect the fabric's surface optical properties (Fig. S32). This is particularly important for the automotive industry, which requires compatibility with a wide range of gloss presentations to meet diverse design needs of product. Moreover, we investigated the sensitivity of the SSF's optical performance to repetitive processes and fabrication parameters, assessing the replicability of its optical properties in repeated manufacturing (Fig. S33). The impact of altering the thickness of the color top layer following the same process was also tested (Fig. S34). The results indicate that the optical performance of the coating is highly replicable for the manufacturing process, and changes in the thickness of the color top layer have a minimal effect on solar reflectance and mid-infrared emissivity. All tests demonstrate the robustness of the manufacturing process in ensuring consistent thermal management performance.

Finally, to quantitatively evaluate the energy-saving potential of SSFs in building and canopy material applications, we selected 14 representative cities across five building climate zones in China and calculated the annual energy savings achieved by different colored SSFs when used as building roofs and envelope structures (Fig. 4j and k), utilizing commercial building energy simulation software EnergyPlus. Detailed information about the calculations and the building model can be found in Text 4 and Table S4. The results show that applying different colored SSFs to building roofs and envelope structures yields significant annual HVAC energy savings, which increase with the solar reflectance of the SSF. Specifically, when used as roofing materials, the annual savings range from 4.68 to 22.30 MJ m^{-2} y^{-1} for black SSFs to 9.30–37.81 MJ m^{-2} y^{-1} for yellow SSFs. When used as both roofs and exterior walls, the savings increase from 4.26 to 37.94 MJ m^{-2} y^{-1} for black SSF to 6.34–63.68 MJ m^{-2} y^{-1} for yellow SSF.

Overall, the colored thermal management fabric with a sandwich structure exhibits excellent thermal management capabilities, along with good compliance, waterproof and antifouling properties, mechanical strength, durability, and adjustable surface gloss. In addition, the SSF demonstrates substantial energy-saving benefits across diverse building applications, effectively combining thermal management performance with color preservation. Compared with methods such as structural coloration, photoluminescence, sprayed pigment coatings, and electrospun nanofiber membranes (Table S5), our SSFs not only exhibit higher near-infrared reflectance and infrared emissivity but also achieve a wide range of color variations from dark to light, demonstrating high color tunability. More importantly, this technology is based on industrial-scale coating and lamination processes, with a simple, environmentally friendly, and highly compatible fabrication process, offering high scalability, mechanical durability, and cost-effectiveness. These advantages highlight the practical feasibility and tremendous potential of our SSFs for real-world applications, which is of great significance for thermal management applications in outdoor functional textiles.

3. Conclusion

In conclusion, we present a sandwich-structured colored thermal management fabric using a simple, cost-effective, environmentally friendly, and scalable way to simultaneously achieve color-preserving radiative cooling and effective latent heat storage, which consists of a near-infrared transparent colored surface layer and a micro-nanostructured radiative cooling layer that strongly reflects NIR light, as well as a phase-change thermal-storage fabric substrate for latent heat storage. Theoretical simulations and calculations, optical characterization, and thermal measurements indicate that the sandwich structure design can reduce solar heat absorption through high NIR reflectivity while delaying temperature increases through effective heat storage. Compared to conventional fabric with the same color, the SSF features an increased NIR reflectivity of up to 0.48. The black/gray/red/blue/yellow SSFs reduced the absorbed solar power by 304.50 $W{\cdot}m^{-2}$/54.86 $W{\cdot}m^{-2}$/306.31 $W{\cdot}m^{-2}$/95.94 $W{\cdot}m^{-2}$/52.33 $W{\cdot}m^{-2}$ under 1000 $W{\cdot}m^{-2}$ solar radiation and were 16.00 °C/9.43 °C/18.04 °C/9.16 °C/8.66 °C cooler than commercial fabrics under strong sunlight. It also provides an enhanced temperature buffering effect during temperature rise, further strengthening color-preserving cooling performance. The synergistic effect of colored radiative cooling and heat-storage properties effectively manages the heat transfer pathways, enabling efficient temperature regulation. Additionally, in various outdoor applications, the temperature management performance significantly outperforms commercial fabrics, achieving “the same color, different thermal performance”. The SSFs also demonstrate excellent practical properties, including flexibility, mechanical strength, environmental adaptability and durability. Through comprehensive heat transfer analysis, this sandwich structure design offers an innovative, sustainable, and scalable solution for color-preserving thermal management to weaken the greenhouse effect and improve thermal comfort. This approach not only holds substantial energy-saving potential but also provides an effective strategy for mitigating heat-related issues.

4. Methods

4.1. Materials

Polyvinyl chloride (PVC) slurry was provided by Benecke-Changshun Auto Trim Zhangjiagang Co., Ltd. TiO_2 (0.2–1 μm) was purchased from Hebei Badu metal materials. Ranbar Black P0086 (black colorant) was purchased from Fine Chemical Company. Conventional colorant (carbon black, red, gray, green) was purchased from BASF SE, and phase change microcapsules were obtained from INNOCAP Company. Polyester/cotton fabrics (100 g/m^2) were provided by Jiangsu Beautiful New Material Co., Ltd.

4.2. Preparation of SSFs

As shown in Fig. S1, the SSF was prepared using the transfer-coating

method. Firstly, phase change microcapsules are formulated into a finishing solution, and the fabric is dipped and padded to undergo multiple dipping processes to achieve the desired loading, resulting in a phase change energy storage fabric substrate. A PVC slurry is compounded with a colorant (2 %) and mixed under vacuum at 2000 rpm for 20 min to create a colored surface coating slurry. This slurry is then coated to a certain thickness on a release paper and placed in a 200 °C oven for 2 min to dry and form a colored surface layer. Subsequently, the PVC slurry is also compounded with a physical foaming agent and a specific mass fraction of TiO_2 nanoparticles, mixed under vacuum at 2000 rpm for 20 min to create a radiative cooling insulating coating slurry. This slurry is coated to a certain thickness on the surface film and dried into a film in a 200 °C oven for 2 min, forming a composite double-layer coating. Finally, this composite is laminated with the phase change energy storage fabric to produce a sandwich-structured colored thermal management fabric (SSF).

4.3. Characterization

The cross-sectional morphology was performed using a Stereo Microscope (NIKON SMZ745T, Japan), and the microscopic morphology of samples was investigated by a field-emission scanning electron microscope (SEM, HITACHI SU8010, Japan).

The reflectance spectral of samples in the sunlight region (0.25–2.5 μm) was measured using a UV–VIS-NIR spectrophotometer (UV3600, Japan) with a polytetrafluoroethylene integrating sphere and a polytetrafluoroethylene plane as standard reflecting pool. The transmission spectra were obtained in the same way, except that the sample was placed at the mouth of the integrating sphere. The average solar reflectance was determined by weighted calculation based on the AM 1.5 solar spectrum, as expressed below:

$$\overline{R} = \frac{\int_{0.25}^{2.5} R(\lambda) I_{AM1.5}(\lambda) d\lambda}{\int_{0.25}^{2.5} I_{AM1.5} d\lambda}$$

where $I_{AM1.5}(\lambda)$ is the ASTM G173-03 global solar intensity spectrum, and $R(\lambda)$ is the sample's spectral reflectance. Ranges 0.4–0.76 μm and 0.76–2.5 μm correspond to the wavelength range used in the calculation of reflectance in the visible and NSWIR wavelengths, respectively.

The spectral emissivity of samples in the mid-infrared wavelength ranges (2.5–20 μm) was tested by an FTIR spectrometer (Nicolet IS50, USA) equipped with a gold integrating sphere. The average emissivity located at the atmosphere window was determined by weighted calculation based on the blackbody radiation function, as expressed below:

$$\overline{\varepsilon} = \frac{\int_{8}^{13} \varepsilon(\lambda) I_{bb}(T, \lambda) d\lambda}{\int_{8}^{13} I_{bb}(T, \lambda) d\lambda}$$

where $I_{bb}(T, \lambda)$ is the spectral intensity emitted by a standard blackbody with a temperature of T, and $\varepsilon(T, \lambda)$ is the sample's spectral emittance.

The chemical structure of samples was analyzed via a Fourier-transformed infrared (FTIR) spectrometer (NICOLET 6700, Thermal Fisher Scientific Company, USA), and the measurement was carried out in the wave number range of 400–4000 cm^{-1}.

The thermal conductivity of samples was measured using thermal constant analyzers (Hot Disk TPS3500, Hot Disk, Sweden). The value was calculated by averaging the values recorded at three different points on the sample surface at 10-min intervals.

The phase change processes of samples were studied by differential scanning calorimetry (DSC, DSC8500, Perkin Elmer Company, USA). The samples were heated or cooled at a rate of 5 °C/min in the 0–50 °C under the N_2 atmosphere. To erase the thermal history, the first heating scan was not recorded.

The thermal stability of samples was evaluated by thermogravimetric analysis (TGA, TGA8000, Perkin Elmer Company, USA). Samples were heated from 50 °C to 800 °C at a heating rate of 10 °C/min under N_2 atmosphere.

The crystallization performance of samples was tested by in-situ X-ray diffractometer (XRD, BRUKER, D8 DISCOVER) with a filtered Cu Kα radiation source (40 kV, 30 mA, λ = 1.54 Å), conducting in the range of diffraction angle 2θ = 5–40°.

The mechanical properties of the samples were measured using a multifunctional electronic fabric strength instrument (YG026MB, China). The rectangle sample fabric with size of 50 mm × 10 mm were stretched at a constant rate of 100 mm·min^{-1}. Each sample was measured repeatedly for three times.

The water contact angle of samples at an ambient temperature was evaluated using optical contact angle measuring and contour analysis systems (OCA15EC, Dataphysics, Germany). The CA value was calculated by averaging the CA values recorded at five different points on the sample surface.

The xenon lamp-accelerated aging test was performed by continuously irradiating the samples under a solar irradiance density of 1000 W/m^2. The UV-accelerated aging test was further determined by means of a QUV accelerated weathering machine. Sample was subjected to the UV irradiance of 0.89 W/m^2 at 340 nm for 8 h at 60 °C, followed by condensation at 50 °C for 4 h with UV lamps off. The optical properties of the sample were evaluated.

4.4. Thermal management performance measurements (indoor and outdoor temperature)

For the indoor temperature measurements, the thermal tests were conducted using the setup (Fig. 3b) for black, gray, red, blue, and yellow samples. The experimental setup is depicted in Fig. 3a–b, with the test chamber dimensions of 200 mm * 200 mm * 100 mm and the fabric dimensions and thickness being 50 mm * 50 mm and 1.3 mm, respectively. The fabric was placed at the center of the upper surface and covered with aluminum foil and polyethylene film to minimize sunlight absorption by the chamber and to reduce the effect of air convection. Xenon lamp was used to simulate solar radiation with various power densities. Thermocouples were utilized to monitor the temperature at the bottom of the sample.

Similarly, for the outdoor temperature measurements, the thermal tests were conducted using the setup in Fig. 3f. For each color, the SSF and commercial samples with an area of 4 cm by 5 cm were placed in a transparent open-top polycarbonate box. A low-density PE film was tautly drawn above the samples as a windshield to reduce the convective heat transfer without substantially hindering solar and thermal infrared transmission. All samples were supported by styrofoam, and the box was placed on another large white styrofoam to reduce the heat transfer between the samples and the ground. The temperature of each sample was measured by a thermocouple pressed to its back face. A thermocouple shielded from sunlight was used to measure air temperature in the box. A pyranometer (TES-1333) was placed beside the sample to measure the direct solar intensity.

4.5. Calculating color from the spectrum

Tristimulus values X, Y, and Z are calculated to measure the response of human eyes to the light based on the CIE color-matching functions $\overline{x}(\lambda)$, $\overline{y}(\lambda)$, and $\overline{z}(\lambda)$ and the sample's reflectance spectrum $R(\lambda)$ using the formulas below [55]

$$X = 100 \frac{\int I(\lambda) R(\lambda) \overline{x}(\lambda) d\lambda}{\int I(\lambda) \overline{y}(\lambda) d\lambda}$$

$$Y = 100 \frac{\int I(\lambda) R(\lambda) \overline{y}(\lambda) d\lambda}{\int I(\lambda) \overline{y}(\lambda) d\lambda}$$

$$Z = 100 \frac{\int I(\lambda) R(\lambda) \overline{z}(\lambda) d\lambda}{\int I(\lambda) \overline{y}(\lambda) d\lambda}$$

Here, CIE Illuminant D65 spectrum I(λ) is used to portray the standard open-air illumination conditions. The chromaticity is then specified by the two normalized values (x and y) derived from the tristimulus values and located in the CIE 1931 color space

$$x = \frac{X}{(X + Y + Z)}$$

$$y = \frac{Y}{(X + Y + Z)}$$

The lightness (L) of the color is calculated by the Lab-XYZ color space conversion

$$L = 116f\left(\frac{Y}{Y_n}\right) - 16$$

where $Y_n = 100$, corresponding to the CIE XYZ tristimulus value of the reference white point under Illuminant D65 and

$$f(t) = \begin{cases} t^{1/3} \text{ if } t > \left(\frac{6}{29}\right)^3 \\ \frac{t}{3 \times \left(\frac{6}{29}\right)^2} + \frac{4}{29} \text{ if } t > \left(\frac{6}{29}\right)^3 \end{cases}.$$

Supplementary data to this article can be found online at https://doi.org/10.1016/j.cej.2025.165702.

CRediT authorship contribution statement

Xuexue Xiang: Writing – original draft, Visualization, Validation, Methodology, Investigation, Formal analysis, Data curation, Conceptualization. **Peida Liu:** Validation, Methodology, Investigation, Formal analysis, Data curation. **Yucan Peng:** Writing – review & editing, Visualization, Supervision, Funding acquisition. **Yao Ma:** Visualization, Supervision, Resources, Project administration, Methodology. **Lijie Du:** Visualization, Supervision, Resources, Methodology. **Jing Gao:** Writing – review & editing, Supervision, Resources, Project administration, Methodology, Funding acquisition, Conceptualization. **Fujun Wang:** Writing – review & editing, Supervision, Resources, Funding acquisition. **Lu Wang:** Writing – review & editing, Supervision, Resources, Project administration, Funding acquisition.

Declaration of competing interest

The authors declare that they have no known competing financial interests or personal relationships that could have appeared to influence the work reported in this paper.

Acknowledgments

The authors gratefully acknowledge the financial support for this research from “the Fundamental Research Funds for the Central Universities CUSF-DH-T-2023047”. Y. P. acknowledges support from National Natural Science Foundation of China (Grant No. 22475007).

Data availability

Data will be made available on request.

References

[1] L. Zhao, X. Lee, R.B. Smith, K. Oleson, Strong contributions of local background climate to urban heat islands, Nature 511 (2014) 216–219, https://doi.org/10.1038/nature13462.
[2] Y. Deng, Y. Yang, Y. Xiao, X. Zeng, H.L. Xie, R. Lan, L. Zhang, H. Yang, Annual energy-saving smart windows with actively controllable passive radiative cooling and multimode heating regulation, Adv. Mater. 36 (2024) 2401869, https://doi.org/10.1002/adma.202401869.
[3] X. Xue, M. Qiu, Y. Li, Q.M. Zhang, S. Li, Z. Yang, C. Feng, W. Zhang, J.G. Dai, D. Lei, W. Jin, L. Xu, T. Zhang, J. Qin, H. Wang, S. Fan, Creating an eco-friendly building coating with smart subambient radiative cooling, Adv. Mater. 32 (2020) 1906751, https://doi.org/10.1002/adma.201906751.
[4] S. Wu, Y. Cao, Y. Li, W. Sun, Recent advances in material engineering and applications for passive daytime radiative cooling, Adv. Opt. Mater. 11 (2022) 2202163, https://doi.org/10.1002/adom.202202163.
[5] M.-C. Huang, M. Yang, X.-J. Guo, C.-H. Xue, H.-D. Wang, C.-Q. Ma, Z. Bai, X. Zhou, Z. Wang, B.-Y. Liu, Y.-G. Wu, C.-W. Qiu, C. Hou, G. Tao, Scalable multifunctional radiative cooling materials, Prog. Mater. Sci. 137 (2023) 101144, https://doi.org/10.1016/j.pmatsci.2023.101144.
[6] R. Liu, S. Wang, Z. Zhou, K. Zhang, G. Wang, C. Chen, Y. Long, Materials in radiative cooling technologies, Adv. Mater. (2024) 2401577, https://doi.org/10.1002/adma.202401577.
[7] G. Smith, A. Gentle, Radiative cooling: energy savings from the sky, Nat. Energy 2 (2017) 17142, https://doi.org/10.1038/nenergy.2017.142.
[8] Y. Zhang, Y. Chen, T. Wang, Q. Zhu, M. Gu, Ultrahigh performance passive radiative cooling by hybrid polar dielectric metasurface thermal emitters, Opto-Electron. Adv. 7 (2024) 230194, https://doi.org/10.29026/oea.2024.230194.
[9] Y. Wu, B. Liu, R. Zhang, Y. Wang, M. Pu, X. Li, X. Luo, Eco-friendly and scalable preparation of high-efficiency passive daytime radiative cooling film based on dual-layer strategy, Adv. Opt. Mater. 13 (2025) 2403087, https://doi.org/10.1002/adom.202403087.
[10] J. Mandal, Y. Fu, A. Overvig, M. Jia, K. Sun, N. Shi, H. Zhou, X. Xiao, N. Yu, Y. Yang, Hierarchically porous polymer coatings for highly efficient passive daytime radiative cooling, Science 362 (2018) 315–319, https://doi.org/10.1126/science.aat9513.
[11] G. Huang, A.R. Yengannagari, K. Matsumori, P. Patel, A. Datla, K. Trindade, E. Amarsanaa, T. Zhao, U. Kohler, D. Busko, B.S. Richards, Radiative cooling and indoor light management enabled by a transparent and self-cleaning polymer-based metamaterial, Nat. Commun. 15 (2024) 3798, https://doi.org/10.1038/s41467-024-48150-2.
[12] D. Li, X. Liu, W. Li, Z. Lin, B. Zhu, Z. Li, J. Li, B. Li, S. Fan, J. Xie, J. Zhu, Scalable and hierarchically designed polymer film as a selective thermal emitter for high-performance all-day radiative cooling, Nat. Nanotechnol. 16 (2021) 153–158, https://doi.org/10.1038/s41565-020-00800-4.
[13] Y. Peng, J.C. Lai, X. Xiao, W. Jin, J. Zhou, Y. Yang, X. Gao, J. Tang, L. Fan, S. Fan, Z. Bao, Y. Cui, Colorful low-emissivity paints for space heating and cooling energy savings, Proc. Natl. Acad. Sci. 120 (2023) 2300856120, https://doi.org/10.1073/pnas.2300856120.
[14] J. Mandal, Y. Yang, N. Yu, A.P. Raman, Paints as a scalable and effective radiative cooling technology for buildings, Joule 4 (2020) 1350–1356, https://doi.org/10.1016/j.joule.2020.04.010.
[15] X. Zhao, T. Li, H. Xie, H. Liu, L. Wang, Y. Qu, S.C. Li, S. Liu, A.H. Brozena, Z. Yu, J. Srebric, L. Hu, A solution-processed radiative cooling glass, Science 382 (2023) 684–691, https://doi.org/10.1126/science.adi2224.
[16] S. Wang, T. Jiang, Y. Meng, R. Yang, G. Tan, Y. Long, Scalable thermochromic smart windows with passive radiative cooling regulation, Science 374 (2021) 1501–1504, https://doi.org/10.1126/science.abg0291.
[17] K. Lin, S. Chen, Y. Zeng, T.C. Ho, Y. Zhu, X. Wang, F. Liu, B. Huang, C.Y.-H. Chao, Z. Wang, C.Y. Tso, Hierarchically structured passive radiative cooling ceramic with solar reflectivity, Science 382 (2023) 691–697, https://doi.org/10.1126/science.adi4725.
[18] Y. Peng, Y. Cui, Advanced textiles for personal thermal management and energy, Joule 4 (2020) 724–742, https://doi.org/10.1016/j.joule.2020.02.011.
[19] S. Zeng, S. Pian, M. Su, Z. Wang, M. Wu, X. Liu, M. Chen, Y. Xiang, J. Wu, M. Zhang, Q. Cen, Y. Tang, X. Zhou, Z. Huang, R. Wang, A. Tunuhe, X. Sun, Z. Xia, M. Tian, M. Chen, X. Ma, L. Yang, J. Zhou, H. Zhou, Q. Yang, X. Li, Y. Ma, G. Tao, Hierarchical-morphology metafabric for scalable passive daytime radiative cooling, Science 373 (2021) 692–696, https://doi.org/10.1126/science.abi5484?rss=1.
[20] R. Wu, C. Sui, T.-H. Chen, Z. Zhou, Q. Li, G. Yan, Y. Han, J. Liang, P.-J. Hung, E. Luo, D.V. Talapin, P.-C. Hsu, Spectrally engineered textile for radiative coolingagainst urban heat islands, Science 384 (2024) 1203–1212, https://doi.org/10.1126/science.adl0653.
[21] E. Pakdel, X. Wang, Thermoregulating textiles and fibrous materials for passive radiative cooling functionality, Mater. Des. 231 (2023) 112006, https://doi.org/10.1016/j.matdes.2023.112006.
[22] P.-C. Hsu, A.Y. Song, P.B. Catrysse, C. Liu, Y. Peng, J. Xie, S. Fan, Y. Cui, Radiative human body cooling by nanoporous polyethylene textile, Science 353 (2016) 1019–1023, https://doi.org/10.1126/science.aaf5471.
[23] Y. Peng, J. Chen, A.Y. Song, P.B. Catrysse, P.-C. Hsu, L. Cai, B. Liu, Y. Zhu, G. Zhou, D.S. Wu, H.R. Lee, S. Fan, Y. Cui, Nanoporous polyethylene microfibres for large-scale radiative cooling fabric, Nat. Sustain. 1 (2018) 105–112, https://doi.org/10.1038/s41893-018-0023-2.
[24] Y. Yang, X. Li, Z. Zhou, Q. Qiu, W. Chen, J. Huang, W. Cai, X. Qin, Y. Lai, Ultrathin, ultralight dual-scale fibrous networks with high-infrared transmittance for high-performance, comfortable and sustainable $PM_{0.3}$ filter, Nat. Commun. 15 (2024) 1586, https://doi.org/10.1038/s41467-024-45833-8.
[25] W.-Z. Song, X.-X. Wang, H.-J. Qiu, N. Wang, M. Yu, Z. Fan, S. Ramakrishna, H. Hu, Y.-Z. Long, Single electrode piezoelectric nanogenerator for intelligent passive daytime radiative cooling, Nano Energy 82 (2021) 105695, https://doi.org/10.1016/j.nanoen.2020.105695.

[26] X. Zhang, W. Yang, Z. Shao, Y. Li, Y. Su, Q. Zhang, C. Hou, H. Wang, A moisture-wicking passive radiative cooling hierarchical metafabric, ACS Nano 16 (2022) 2188–2197, https://doi.org/10.1021/acsnano.1c08227.
[27] P. Yao, Z. Chen, T. Liu, X. Liao, Z. Yang, J. Li, Y. Jiang, N. Xu, W. Li, B. Zhu, J. Zhu, Spider-silk-inspired nanocomposite polymers for durable daytime radiative cooling, Adv. Mater. 34 (2022) 2208236, https://doi.org/10.1002/adma.202208236.
[28] H. Yuan, R. Liu, S. Cheng, W. Li, M. Ma, K. Huang, J. Li, Y. Cheng, K. Wang, Y. Yang, F. Liang, C. Tu, X. Wang, Y. Qi, Z. Liu, Scalable fabrication of dual-function fabric for zero-energy thermal environmental management through multiband, synergistic, and asymmetric optical modulations, Adv. Mater. 35 (2023) 2209897, https://doi.org/10.1002/adma.202209897.
[29] S. Zhong, L. Song, W. Ren, W. Liu, S. Yuan, T. Xu, L. Xu, J. Zhang, Y. Cai, L. Yi, Radiative cooling cellulose-based fabric with hierarchical structure for outdoor personal thermal management, Chem. Eng. J. 489 (2024) 151482, https://doi.org/10.1016/j.cej.2024.151482.
[30] N. Cheng, Z. Wang, Y. Lin, X. Li, Y. Zhang, C. Ding, C. Wang, J. Tan, F. Sun, X. Wang, J. Yu, B. Ding, Breathable dual-mode leather-like nanotextile for efficient daytime radiative cooling and heating, Adv. Mater. (2024) 2403223, https://doi.org/10.1002/adma.202403223.
[31] J. Dong, Y. Peng, Y. Zhang, Y. Chai, J. Long, Y. Zhang, Y. Zhao, Y. Huang, T. Liu, Superelastic radiative cooling metafabric for comfortable epidermal electrophysiological monitoring, Nano-Micro Lett. 15 (2023) 181, https://doi.org/10.1007/s40820-023-01156-9.
[32] C. Fan, Y. Zhang, Z. Long, A. Mensah, Q. Wang, P. Lv, Q. Wei, Dynamically tunable subambient daytime radiative cooling metafabric with janus wettability, Adv. Funct. Mater. (2023) 2300794, https://doi.org/10.1002/adfm.202300794.
[33] Y. Xu, X. Zhang, Y. Li, Y. Zhang, T. Zhao, Y. Zeng, Radiative cooling face mask based on mixed micro- and nanofibrous fabric, Chem. Eng. J. 481 (2024), https://doi.org/10.1016/j.cej.2024.148722.
[34] X. Yin, R. Yang, G. Tan, S. Fan, Terrestrial radiative cooling using the cold universe as a renewable and sustainable energy source, Science 370 (2020) 786–791, https://doi.org/10.1126/science.abb0971.
[35] D. Sood, D. Das, S. Fatima Ali, D. Rakshit, Numerical analysis of an automobile cabin thermal management using passive phase change material, Ther. Sci. Eng. Prog. 25 (2021) 100870, https://doi.org/10.1016/j.tsep.2021.100870.
[36] E. Oró, E. de Jong, L.F. Cabeza, Experimental analysis of a car incorporating phase change material, J. Energy Storage 7 (2016) 131–135, https://doi.org/10.1016/j.est.2016.05.003.
[37] A. Afzal, C.A. Saleel, I.A. Badruddin, T.M.Y. Khan, S. Kamangar, Z. Mallick, O. D. Samuel, M.E.M. Soudagar, Human thermal comfort in passenger vehicles using an organic phase change material — an experimental investigation, neural network modelling, and optimization, Build. Environ. 180 (2020) 107012, https://doi.org/10.1016/j.buildenv.2020.107012.
[38] I.M.A. Aljubury, A.A. Farhan, M.A. Mussa, Experimental study of interior distribution inside parked automobile cabin, J. Eng. (2015) 21, https://doi.org/10.31026/j.eng.2015.03.01.
[39] B. Xie, Y. Liu, W. Xi, R. Hu, Colored radiative cooling: progress and prospects, Mater. Today Energy 34 (2023) 101302, https://doi.org/10.1016/j.mtener.2023.101302.
[40] H. Xing, X. Shu, B. Hong, N. Wang, W. Wang, G.P. Wang, Recent progress in color-preserving radiative cooling: multispectral control in visible and infrared wavelength, Mater. Today Phys. 38 (2023) 101242, https://doi.org/10.1016/j.mtphys.2023.101242.
[41] W. Li, Y. Shi, Z. Chen, S. Fan, Photonic thermal management of coloured objects, Nat. Commun. 9 (2018) 4240, https://doi.org/10.1038/s41467-018-06535-0.
[42] H. Luo, Q. Li, K. Du, Z. Xu, H. Zhu, D. Liu, L. Cai, P. Ghosh, M. Qiu, An ultra-thin colored textile with simultaneous solar and passive heating abilities, Nano Energy 65 (2019) 103998, https://doi.org/10.1016/j.nanoen.2019.103998.
[43] M. Kong, X. Guo, S. Zhang, Y. Zhang, B. Tang, Structural colored textiles with high color visibility and stability for intelligent thermoregulating performance, Chem. Eng. J. 473 (2023) 145332, https://doi.org/10.1016/j.cej.2023.145332.
[44] X. Li, H. Xu, Y. Yang, F. Li, S. Ramakrishna, J. Yu, D. Ji, X. Qin, Selective spectral absorption of nanofibers for color-preserving daytime radiative cooling, Mater. Horiz. 10 (2023) 2487–2495, https://doi.org/10.1039/D3MH00391D.
[45] B.Y. Liu, J. Wu, C.H. Xue, Y. Zeng, J. Liang, S. Zhang, M. Liu, C.Q. Ma, Z. Wang, G. Tao, Bioinspired superhydrophobic all-in-one coating for adaptive thermoregulation, Adv. Mater. 36 (2024) 2400745, https://doi.org/10.1002/adma.202400745.
[46] J. Zhang, S. Xu, Y. Cai, L. Yi, Colorfully coated cotton fabric for passive daytime radiative cooling, Prog. Org. Coat. 182 (2023) 107678, https://doi.org/10.1016/j.porgcoat.2023.107678.
[47] C. Wang, H. Chen, F. Wang, Passive daytime radiative cooling materials toward real-world applications, Prog. Mater. Sci. 144 (2024) 101276, https://doi.org/10.1016/j.pmatsci.2024.101276.
[48] T.B. Freeman, K.E.O. Foster, C.J. Troxler, C.W. Irvin, A. Aday, S.K.S. Boetcher, A. Mahvi, M.K. Smith, A. Odukomaiya, Advanced materials and additive manufacturing for phase change thermal energy storage and management: a review, Adv. Energy Mater. 13 (2023) 2204208, https://doi.org/10.1002/aenm.202204208.
[49] J. Shi, M. Qin, W. Aftab, R. Zou, Flexible phase change materials for thermal energy storage, Energy Storage Mater. 41 (2021) 321–342, https://doi.org/10.1016/j.ensm.2021.05.048.
[50] M.Q. Wu, S. Wu, Y.F. Cai, R.Z. Wang, T.X. Li, Form-stable phase change composites: preparation, performance, and applications for thermal energy conversion, storage and management, Energy Storage Mater. 42 (2021) 380–417, https://doi.org/10.1016/j.ensm.2021.07.019.
[51] M. Yang, H. Zhong, T. Li, B. Wu, Z. Wang, D. Sun, Phase change material enhanced radiative cooler for temperature-adaptive thermal regulation, ACS Nano 17 (2023) 1693–1700, https://doi.org/10.1021/acsnano.2c11916.
[52] M. Qin, K. Jia, A. Usman, S. Han, F. Xiong, H. Han, Y. Jin, W. Aftab, X. Geng, B. Ma, Z. Ashraf, S. Gao, Y. Wang, Z. Shen, R. Zou, High-efficiency thermal-shock resistance enabled by radiative cooling and latent heat storage, Adv. Mater. 36 (2024) 2314130, https://doi.org/10.1002/adma.202314130.
[53] Y. Tao, J. Zhang, Poriferous PVC materials with high daytime radiation cooling property fabricated by etching SBS as template, Mater. Lett. 304 (2021) 130675, https://doi.org/10.1016/j.matlet.2021.130675.
[54] H. Chen, Z. Yue, D. Ren, H. Zeng, T. Wei, K. Zhao, R. Yang, P. Qiu, L. Chen, X. Shi, Thermal conductivity during phase transitions, Adv. Mater. 31 (2019) 1806518, https://doi.org/10.1002/adma.201806518.
[55] Y. Chen, J. Mandal, W. Li, A. Smith-Washington, C. Tsai, W. Huang, S. Shrestha, N. Yu, R.P.S. Han, A. Cao, Y. Yang, Colored and paintable bilayer coatings with high solar-infrared reflectance for efficient cooling, Sci. Adv. 6 (2020) eaaz5413, https://doi.org/10.1126/sciadv.aaz5413.